Arabian Journal of Geosciences (2020) 13: 1215
https://doi.org/10.1007/s12517-020-06237-2

ORIGINAL PAPER

Numerical simulation of the coal temperature field evolution under the liquid nitrogen cold soaking

Shumin Liu[1] · Xuelong Li[1,2,3,4] · Dengke Wang[2]

Received: 7 August 2020 / Accepted: 1 November 2020 / Published online: 12 November 2020

Abstract

Liquid nitrogen fracturing technology is largely based on the characteristics of coal and rock destruction caused by its low temperature to achieve the purpose of increasing permeability. The temperature field study is very important in liquid nitrogen cold soaking. In order to study the spatiotemporal characteristics of the internal temperature field inside coal under the liquid nitrogen cold soaking, the overall heat transfer law of coal is discussed. Based on the theory of heat transfer, this paper discusses the heat transfer equation of coal under the liquid nitrogen cold soaking. A cold shock simulation experiment is performed on the coal specimens during the liquid nitrogen cold soaking by the COMSOL software, and the temperature field change of the coal specimens during the liquid nitrogen cold soaking are obtained. In addition, the simulation results are compared with the experimental results of coal specimens under the liquid nitrogen cold soaking to verify the rationality of the theory and simulation analysis. The results show that the temperature field of coal specimens propagates in the form of waves under the liquid nitrogen cold soaking, which gradually decrease with increasing distance. The closer the dried coal specimens are to the liquid nitrogen boundary surface, the greater the temperature impact speed and the shorter the time required to reach a steady state. Both the surface of the coal specimen and its internal temperature change curve can be divided into three typical phases: the accelerated cooling phase, the decelerated cooling phase, and the low-temperature maintenance phase. The laboratory test results have a good correspondence with the numerical simulation results, which show that it is feasible to use numerical simulation to study the temperature field change law of coal and rock under liquid nitrogen cold soaking.

Keywords Coal · Liquid nitrogen cold soaking · Numerical simulation · Temperature field evolution

Introduction

The coal industry is the basic industry of China's national economy, and as an important strategic resource of the country, coal occupies a dominant position in China's primary energy consumption (Zhang et al. 2014; Kong et al. 2020; Yang et al. 2019; Zhou et al. 2020). Coalbed methane (CBM) is not only a major disaster source for coal mines in China, but also a non-renewable unconventional energy source and a strong greenhouse gas (Mitra et al. 2012; Liu et al. 2019; Xue et al. 2020). Fifty percent to 70% of coal seams in China's coal mines belong to high gas seams. It currently extends downward at a mining speed of 10~20 m per year. With the increase of mining depth, the coal seam geology and occurrence conditions become more and more complex, which lead to the increase of coal seam pressure and gas pressure, coal and gas outburst, and coal seam gas explosion and other gas disasters becoming increasingly serious (Moore 2012; Perera and Ranjith 2012; Mark and Gauna 2016).

The efficient extraction and utilization of gas can not only ensure the safe production of coal mines, but can also beneficially change China's energy structure (Huang et al. 2012; Kong et al. 2019; Zhang et al. 2020). At present, technologies

Responsible Editor: Murat Karakus

✉ Xuelong Li
lixlcumt@126.com

[1] State Key Laboratory of Coal Mine Disaster Dynamics and Control, Chongqing University, Chongqing 400044, China

[2] State Key Laboratory Cultivation Base for Gas Geology and Gas Control, Henan Polytechnic University, Jiaozuo 454150, Henan, China

[3] College of Energy and Mining Engineering, Shandong University of Science and Technology, Qingdao 266590, China

[4] Mine Disaster Prevention and Control-Ministry of State Key Laboratory Breeding Base, Shandong University of Science and Technology, Qingdao 266590, China

such as deep-hole blasting pre-splitting, hydraulic fracturing, and hydraulic slitting are mainly used to increase the permeability of coal and rock (Lin et al. 2015; Yin et al. 2015; Li et al. 2018; Lu et al. 2019). The application of these re-enhancement technologies has increased the permeability of the coal seam, promoted the rapid development of the CBM industry, and effectively restrained the occurrence of coal mine gas disasters. However, hydraulic measures are used to consume large amounts of water, and some chemical reagents contained in the fracturing fluid will cause pollution to water resources and the environment. Therefore, it is necessary to find an effective dehydration fracturing technology to solve the problems existing in the above re-enhancement measures.

In recent years, many scholars have begun to explore and develop new anhydrous fracturing re-enhancement technologies, such as injecting cryogenic liquid nitrogen fluid into coal and rock, and applying them to in coal seam re-enhancement field (Mcdaniel et al. 1997; Coetzee et al. 2014; Cha et al. 2014; Cai et al. 2016; Li et al. 2016). The core idea of liquid nitrogen fracturing is to use liquid nitrogen to generate huge gas pressure in a limited space, prompting the initiation of cracks in coal seams, expanding and connections, forming a crack network, and increasing the permeability of coal seams (Qin et al. 2017; Shang et al. 2018; Liu et al. 2020a, b). The change of the pore and crack structure of coal and rock under the liquid nitrogen cold soaking is the result of multiphysics coupling (Karacan et al. 2011). Among them, the temperature field change is the basic problem for studying multiphysics coupling (Hebblewhite and Galvin 2017). For different temperatures and different coal materials, the effect will be different, and the internal heat conduction law is complex and changeable (Chaudhary and Li 2014). Ramey (1962) performed simulation calculations of the wellbore temperature field. In order to simplify the model, the research object was regarded as a single-phase incompressible fluid and a single-phase ideal gas. Formation fluids were ignored in the study, and only fluid flow in the tubing casing was considered. Finally, the famous Ramey model suitable for vertical wells was established. Settari and Cleary (1984) considered the effects of heat transfer along the fracture length and fracture height, the heat loss generated by fracturing fluid filtration, and the heat transfer between the fracturing fluid in the fracture and the fracture wall and established a corresponding calculation model. The model was basically the same as the actual situation, but the calculation process was quite complicated. Benaceur and Stephenson (2010) treated the formation as an infinite solid with a uniform initial temperature. Regardless of the temperature difference of the fracturing fluid in the crack, it was assumed that heat exchange occurred only in the vertical direction of the crack surface, and the thermal penetration depth was defined. Finally, the temperature distribution of the fluid in the crack was calculated. Based on the extremely low temperature of liquid nitrogen (77.15 K), after liquid nitrogen was injected into the rock, the low-temperature exchanges with the surrounding medium and a certain temperature gradient were gradually formed in the rock. The study by Cha et al. (2014) showed that the temperature gradient generated by the liquid nitrogen can cause cracks in the rock and change the crack structure of the rock. The low-temperature characteristics of liquid nitrogen caused the rock skeleton to contract drastically and break, resulting in a large number of micro-cracks. Park et al. (2004) carried out research on the influencing factors of rock's thermophysical parameters and their relationship with temperature field. The results showed that the specific heat capacity and thermal expansion coefficient of the rock decreased with the decrease of temperature when the temperature of the rock changed between 313.15 and 113.15 K, while the thermal conductivity had little effect on the change of temperature. Mottaghy and Rath (2006) considered the effect of phase transition on temperature. The migration of unfrozen water and the concentration of solutes in porous media under frozen conditions directly affected temperature transfer. In order to study the heat conduction law of rocks in freeze-thaw environments, Shen et al. (2018) and McDermott et al. (2006) embedded temperature sensors into sandstone samples in advance and monitored the temperature change of different positions inside the samples during freezing. Guo and Liu (2014) placed the temperature measurement element inside the rock sample and used a combination of experiments and numerical analysis to study the temperature equilibrium law of the rock in the freeze-thaw environment. Bronfenbrenerb (2009) used a low-temperature constant temperature bath to provide the required ambient temperature of the soil sample, inserted a temperature sensor into the soil sample center to monitor the soil sample temperature in real time, and conducted experimental research on soil freezing temperature and subcooling temperature under different cooling conditions. Regarding the study of the thermal conductivity of coal and rock in low-temperature environments, Vitelv et al. (2015) explored the characteristics of the influence of frozen pipes on the temperature of surrounding rock masses by using the artificial freezing method based on thermal conduction theory and numerical simulation analysis. Zhang et al. (2015) used the sensible heat capacity method to transform the phase transition Stefan problem caused by the freezing temperature field into a single-phase nonlinear transient heat conduction problem in the same region. The finite element method was used to explore the evolution of freezing temperature field in artificial frozen mine shaft. Tan et al. (2011) and Taron et al. (2009) divided the low-temperature process into a frozen area and an unfrozen area based on the location of the frozen peak surface and analyzed the temperature field using a variable substitution method. The relationship between the frozen peak surface radius and the freezing time was obtained, and the exponential integral

function was used to represent the temperature of the frozen and unfrozen regions. Yang (2001) used CT scanning test technology to conduct detailed studies on the meso-damage propagation mechanism, water migration, ice formation, and changes in damage structure within the coal under different freezing temperatures. Shi et al. (2019) did some field tests and simulations to investigate quantitatively the distribution of goaf temperature under the injection of liquid nitrogen. It was observed that a low-temperature cooling zone due to injection of liquid nitrogen gradually grew and became relatively stable 90 min after continuous injection. The size of the cooling zone depended on the injection location and flow rate. The above research has a good guiding value for understanding the heat conduction law of coal and rock under low-temperature conditions. However, due to the limitation of observation and analysis methods, the analysis results do not give the internal temperature evolution law of coal and rock, and the temperature change during the liquid nitrogen cold soaking is an important evaluation index of the physical and mechanical properties of coal and rock.

Based on the concept of liquid nitrogen-induced cracked coal and rock, a physical model of the temperature field of coal under the liquid nitrogen cold soaking was established. The COMSOL Multiphysics software was used to numerically simulate coal parameters based on coal parameters to analyze the internal temperature field of coal during the liquid nitrogen cold soaking. Comparing the simulation results with the experimental results, the theoretical analysis was well verified. This study will provide a reference for the study of the internal temperature field of coal and rock during the liquid nitrogen cold soaking. The research results are of great significance to reveal the mechanism of liquid nitrogen fracturing and improve and optimize the liquid nitrogen fracturing technology.

Temperature field model of liquid nitrogen cold soaking coal

Basic assumptions

Coal and rock is a typical complex organic material composed of a variety of minerals. During liquid nitrogen cold soaking, a variety of materials inside the coal and rock have different thermal effects, which restrict and influence each other. Therefore, the liquid nitrogen cold soaking process is a quite complicated process. This paper assumes that coal specimens are dry coal samples and are only affected by temperature fields. In addition, the following assumptions are made on the model: (1) The coal is isotropic and does not undergo phase changes. (2) The initial temperature of the coal is uniform. (3) In the process of the liquid nitrogen cold soaking coal, heat convection and heat radiation are ignored, and only heat conduction is considered. (4) The temperature change process of coal under the liquid nitrogen cold soaking satisfies local thermal equilibrium.

Coal transient heat conduction model

According to the theory of heat transfer, the transient temperature field equation of the coal cylinder is obtained from the energy conservation law (Incropera and DeWitt 1996; Holman 1990):

$$\rho c\frac{\partial T}{\partial \tau}+Q=\frac{\partial}{\partial x}\left(k\frac{\partial T}{\partial x}\right)+\frac{\partial}{\partial y}\left(k\frac{\partial T}{\partial y}\right)+\frac{\partial}{\partial z}\left(k\frac{\partial T}{\partial z}\right) \quad (1)$$

The geometry of the coal cylinder and the liquid nitrogen cold soaking are symmetrical to the central axis of the cylinder. Therefore, this problem belongs to the problem of spatial axisymmetric, and the continuous injection of liquid nitrogen into the coal through the center hole of the coal sample causes the coal sample to undergo volume deformation, and the thermal power Q is generated inside the coal, that is the equation (2)

$$Q=\beta T_0\frac{\partial \varepsilon_v}{\partial \tau} \quad (2)$$

In the formula, ε_v is the volume strain of the coal test piece. T_0 is the initial temperature of the coal (K). $\beta=\alpha E/3(1-2\mu)$, where α is the coefficient of linear thermal expansion (1.6×10^{-5} 1/K). τ is the liquid nitrogen cold soak time (s).

Therefore, Eq. (1) can be simplified as:

$$\rho c\frac{\partial T}{\partial \tau}+\beta T_0\frac{\partial \varepsilon_v}{\partial \tau}=2\frac{\partial}{\partial x}\left(k\frac{\partial T}{\partial x}\right)+\frac{\partial}{\partial z}\left(k\frac{\partial T}{\partial z}\right) \quad (3)$$

where ρ is the density of coal (kg/m^3). c is the specific heat capacity of coal (kJ/(kg·K)). k is the thermal conductivity of coal (W/(m·K)). T is the instantaneous temperature of the coal (K). τ is the liquid nitrogen cold soak time (s). x is the radius of the coal specimen (m). z is the height of the coal specimen (m).

The specific simulation boundary conditions are as follows:

For the first type of boundary conditions, take the temperature as a fixed value that is expressed by Eq. (4)

$$T_1=C \quad (4)$$

For the third type of boundary conditions, the surface heat transfer coefficient of coal specimens on a given boundary is h and the fluid (liquid nitrogen) temperature is T_f, that is,

$$-\left.\frac{\partial T}{\partial n}\right|_{r=0}=h\left(T_\tau-T_f\right) \quad (5)$$

From the comprehensive Eqs. (4) and (5), it can be concluded that the physical model of coal temperature field under the liquid nitrogen cold soaking is as follows:

$$\begin{cases} \rho c = \dfrac{\partial T}{\partial \tau} + \beta T_0 \dfrac{\partial \varepsilon_v}{\partial \tau} = 2\dfrac{\partial}{\partial x}\left(k\dfrac{\partial T}{\partial x}\right) + \dfrac{\partial}{\partial z}\left(k\dfrac{\partial T}{\partial z}\right), \\ \qquad (0 < x < r_0, 0 < z < b) \\ T(x,z,\tau)|_{\tau=0} = T_0, \quad (0 < x < r_0, 0 < z < b), \\ -\left.\dfrac{\partial T}{\partial z}\right|_{\tau=0} = 0, \quad (0 < z < b) \\ -\left.\dfrac{\partial T}{\partial x}\right|_{\tau=0} 0, \quad (z = 0, b) \end{cases} \tag{6}$$

where T is the instantaneous temperature of coal (K). C is a constant. $\boldsymbol{n}$ is the outer normal length of the heat transfer surface of the coal specimen. h is the heat transfer coefficient of the coal surface (W/(m^2·K). T_0 is the initial temperature of the coal (K). T_f is the fluid (liquid nitrogen) temperature (K). r_0 is the maximum radius of the coal specimen (m). b is the maximum height of the coal specimen (m).

Establishment of finite element model of coal under liquid nitrogen cold soaking

The COMSOL Multiphysics software is large-scale multiphysics direct coupling analysis software. It is widely used in scientific research and engineering calculation in various fields. The COMSOL Multiphysics software has a unique design concept, which abandons the concept of a single-element stiffness matrix when meshing and directly assembles multiple partial differential equations (groups) into a total stiffness matrix. The result of this is that no matter how many physics are solved, the users only need to select the corresponding partial differential equations for any combination, and the software automatically solves them simultaneously, realizing direct, two-way real-time coupling of any physics. COMSOL Multiphysics achieves highly accurate numerical simulation with efficient computing performance and multi-field bidirectional direct coupling analysis capabilities.

Model building

The simulation object is a cylindrical coal specimen with a diameter of 0.05 m and a height of 0.1 m. The coordinate origin (0, 0, 0) is located at the bottom surface center of the cylinder. Drill the hole along the z-axis. The diameter of the borehole is 0.006 m, and the depth is 0.055 m. The center position coordinates of the borehole bottom are (0, 0, 0.045), as shown in Fig. 1a. Since the boundary conditions of the model meet the axisymmetric conditions, one quarter of the three-dimensional model is used for research. In order to facilitate the study of the temperature field distribution of coal, the monitoring points 1~11 and the distance between adjacent monitoring points are arranged on the coal specimen, as shown in Fig. 1b. Monitoring point 2 is the middle point of monitoring points 1 and 3, monitoring point 6 is the middle point of monitoring points 5 and 7, and monitoring point 7 is located at the middle point of monitoring points 6 and 8.

Parameter selection

The temperature boundary conditions are as follows: the initial temperature is 293.15 K; the liquid nitrogen surrounds the entire cylindrical surface of the coal specimen; the cylindrical surface temperature of the coal specimen is 77.15 K; the upper and lower end surfaces; and the drilling surface are flux boundaries. The heat can continue to be transmitted outward through these surfaces. In order to simplify the model, the thermodynamic parameters (elastic modulus, thermal expansion coefficient, and Poisson's ratio) of the coal are taken as constants, and the values are referenced (Wang et al. 2017; Shu et al. 2020). The simulation parameters used in this study are presented in Table 1.

Liquid nitrogen cold leaching coal simulation experiment scheme

The initial temperature of the coal specimen is 293.15 K, and the liquid nitrogen cold soaking temperature is 77.15 K. The simulation scheme is as follows: the coal specimen is placed in the center of the annular cavity filled with liquid nitrogen, and the cylindrical surface temperature of the coal specimen is 77.15 K. The upper and lower bottom surfaces and drilled surfaces of the coal specimen are flux boundaries. Taking the center bottom surface of the coal specimen as the coordinate's origin, the XOZ section is selected as the research object, and 11 monitoring points are set on this plane. The coordinates of monitoring points 1–11 are (0.003, 0, 0.1), (0.003, 0, 0.0725), (0.003, 0, 0.045), (0, 0, 0.045), (0, 0, 0.02), (0.00625, 0, 0.02), (0.0125, 0, 0.02), (0.01875, 0, 0.02), (0.0125, 0, 0.04), (0.0125, 0, 0.06), and (0.0125, 0, 0.08), and specific positional relationships are shown in Fig. 1b.

Meshing and solving settings

Meshing is an important part of numerical calculation. The quality of the meshing directly affects the fineness of the entire model calculation process. This model is three-dimensional axisymmetric, and the axis of symmetry is the z-axis. The triangle mesh in the mesh drawing function of the COMSOL Multiphysics version 3.5a software is used to divide, and the mesh consists of 10662 elements. The final geometric model meshing is shown in Fig. 2.

Transient studies are added in COMSOL Multiphysics version 3.5a. The liquid nitrogen cold soaking time is set to 3 h, and the time interval is set to 60 s. Parameterized scanning is used to solve the temperature field distribution of coal under the liquid nitrogen cold soaking.

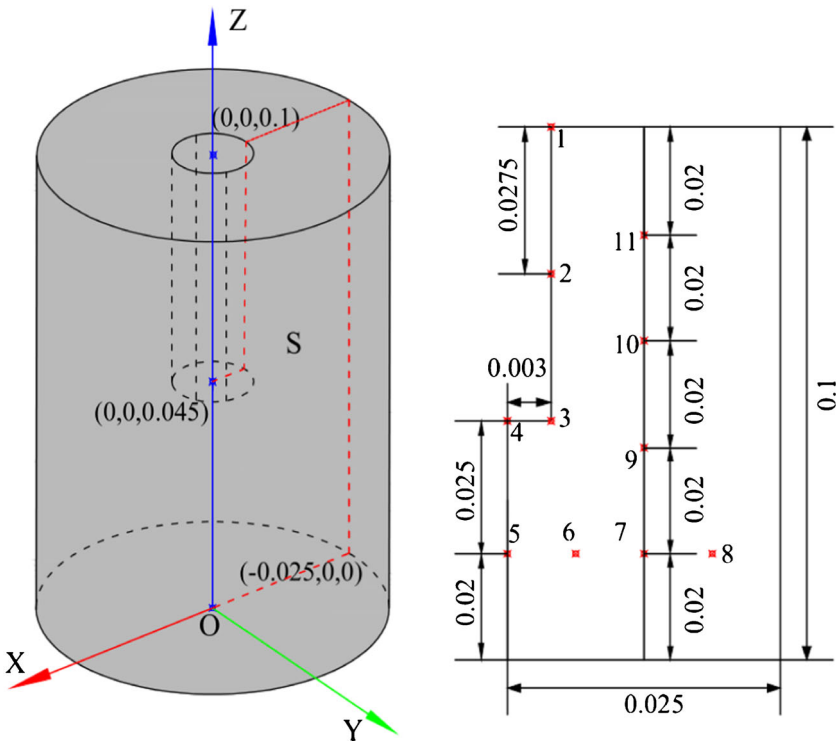

(a) Physical model (b) Sectional view

Fig. 1 The coal physical model of numerical calculation (m)

Results and discussion

Overall change law of coal temperature field under liquid nitrogen cold soaking

In the process of fracturing coal and rock by liquid nitrogen, the problem of temperature field change of coal and rock is involved. Therefore, the study of the temperature field is the most important information point of liquid nitrogen induced cracked coal and rock. In the following, the internal temperature field distributions of coal during the liquid nitrogen cold soaking for 600 s, 1200 s, and 3600 s are taken as an example for analysis and discussion. Cloud diagrams of coal internal

Table 1 Model parameters

Variable (units)	Value	Remark
E (GPa)	3.2	Young's modulus of coal
μ (1)	0.32	Poisson's ratio of coal
ρ (kg/m^3)	1550	Density of coal
C_p (kJ/kg K)	1.349	Specific heat capacity
k (W/m K)	0.26	Thermal conductivity
h (W/m^2 K)	5	Convective heat transfer coefficient
α (1/K)	1.6E−6	Thermal expansion coefficient
T_0 (K)	293.15	Initial temperature
T_f (K)	77.15	Liquid nitrogen temperature

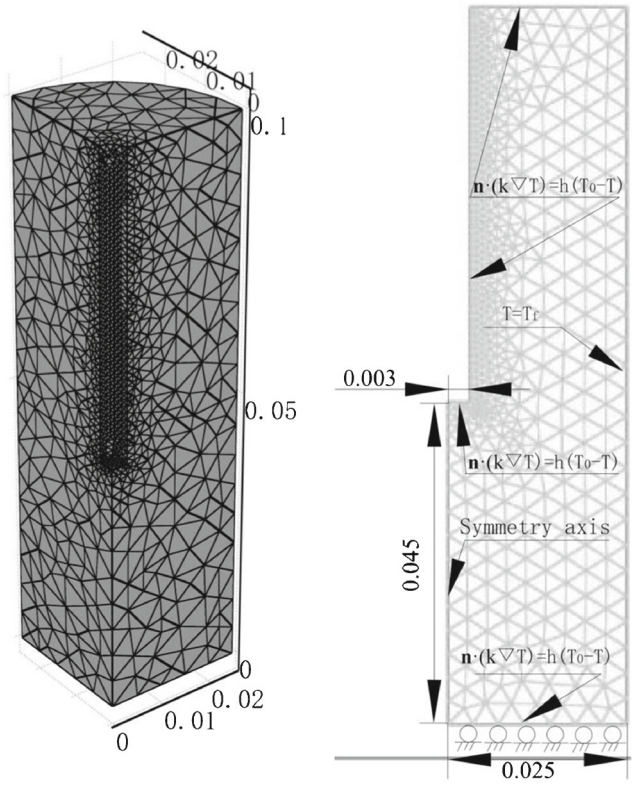

(a) Geometry mesh (b) boundary conditions

Fig. 2 Geometry of mesh and boundary conditions of the numerical model

temperature field distribution at different liquid nitrogen cold soaking time are shown in Fig. 3.

It can be known from Fig. 3 that the temperature fields of coal under the liquid nitrogen cold soaking all propagate in a wave form from the cylindrical wall of the coal specimen to the center of the coal specimen at a certain speed. The longer the liquid nitrogen cold soaking time is, the larger the temperature field spreads. The temperature of the point where the cold shock wave propagates will suddenly decrease until it finally stabilizes. The temperature field cloud diagram in Fig. 3 can only see the distribution cloud map of the temperature field at a specific time, and it is not obvious to see the law of temperature change with time.

Take monitoring points 7, 9, 10, and 11 for temperature changes as shown in Fig. 4. Under the conditions of liquid nitrogen cold soaking, the temperature of coal has a negative logarithmic function curve. The positions of the four monitoring points are equidistant from the cylinder surface of the coal specimen. With the increase of liquid nitrogen cold soaking time, the temperature is divided into three phases: Phase I, when $t < 240$ s, the temperature of the four monitoring points decreases rapidly with the liquid nitrogen cold soaking time. When $t = 240$ s, the maximum temperature impact speed is − 0.23 K/s. Phase II, when 240 s < t < 3900 s, the temperature of the four monitoring points decelerated and decreased with the increase of the liquid nitrogen cold soaking time. When t = 3900 s, the temperature impact speed tends to zero. Phase III, when $t > 3900$ s, the temperature at the four monitoring points is maintained at a low temperature, that is, the temperature field of the coal sample reaches dynamic equilibrium.

The radial temperature gradients of monitoring points 7, 9, 10, and 11 along the time are shown in Fig. 5. It can be seen from Fig. 5 that when the initial temperature of coal is 273.15 K, the temperature gradients at monitoring points 7, 9, 10, and 11 have the largest negative phase at $t = 240$ s. The maximum temperature gradient at monitoring point 7 is − 552.79 K/m. The maximum temperature gradient at monitoring point 9 is − 555.68 K/m. The maximum temperature gradients at monitoring points 10 and 11 are − 572.63 K/m and − 553.95 K/m, respectively. The temperature gradient of coal along the radial direction under liquid nitrogen cold soaking can be divided into three changing stages with time: increasing temperature gradient (I), decreasing temperature gradient (II), and constant temperature gradient (III).

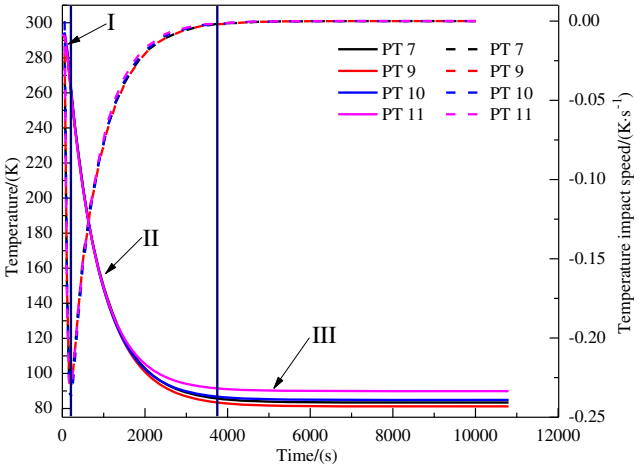

Fig. 4 Changes in coal temperature with the liquid nitrogen cold soaking time

Variation of temperature field coal surface under liquid nitrogen cold soaking

The temperature and temperature impact speed of coal surface monitoring points 1, 2, and 3 over time are shown in Fig. 6. It can be seen from Fig. 6 that when $t < 2400$ s, as the liquid nitrogen cold soaking time increases, the temperatures at monitoring points 1~3 all decrease rapidly. When the temperature at monitoring point 1 drops to 138.77 K, the temperature at monitoring point 2 drops to 103.00 K, and when the temperature at monitoring point 3 drops to 92.33 K, the temperature at monitoring points 1~3 remains stable. The

(a) t=600 s (b) t=1200 s (c) t=3600 s

Fig. 3 Cloud diagram of temperature field inside coal section under different liquid nitrogen cold soaking time

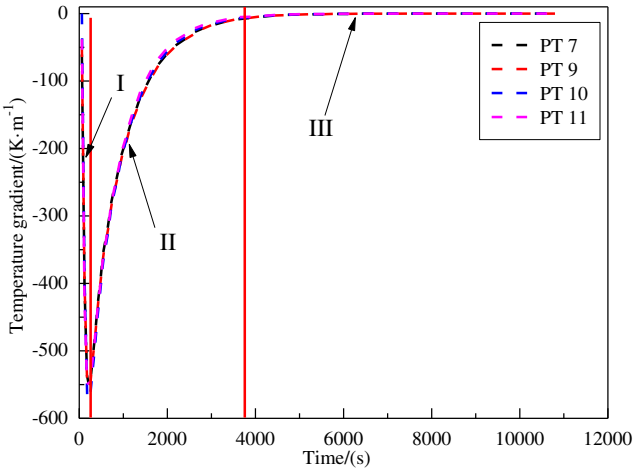

Fig. 5 Changes in temperature impact speed of coal with the liquid nitrogen cold soaking time

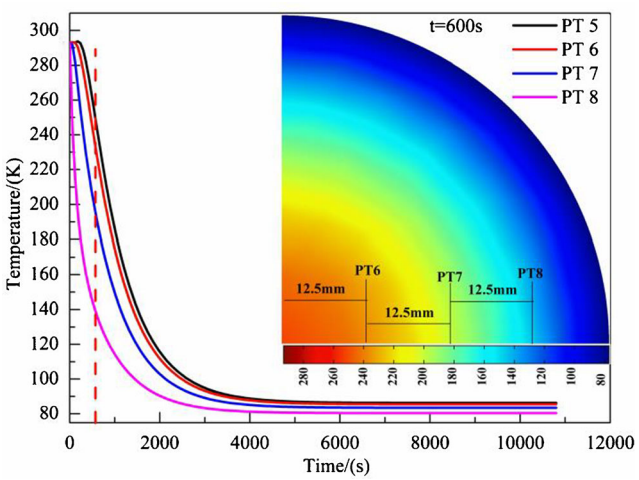

Fig. 7 Axial temperature changes of coal with the liquid nitrogen cold soaking time

temperature impact speed of coal under the liquid nitrogen cold soaking shows an increase first and then a decrease with time and eventually changes to zero. The coal surface has different temperature impact speeds at different locations at the same time. When $t > 480$ s, with the increase of the liquid nitrogen cold soaking time, the coal surface temperature accelerates and decreases. The temperature impact speeds of monitoring points 1, 2, and 3 reach the maximum at 480 s, and the maximum temperature impact speed of monitoring point 1 is − 8.57 K/s. The maximum temperature impact speed of monitoring points 2 and 3 are − 10.00 K/s and − 9.71 K/s, respectively. The surface temperature of coal decreases with the increase of the liquid nitrogen cold soaking time, but the decreasing speed becomes slower and gradually stabilizes.

Variation of temperature field inside coal under liquid nitrogen cold soaking

Under the conditions of liquid nitrogen cold soaking, the temperature of coal decreases with time. The monitoring points 5~8 is taken as the research object. The temperature change of monitoring points 5~8 with time under the liquid nitrogen cold soaking is shown in Fig. 7. In the temperature range study, when the initial temperature is 293.15 K, the temperature at monitoring point 8 closest to the cold impact wave source decreases fastest with the liquid nitrogen cold soak time. At t = 4200 s, the temperature at monitoring point 8 drops to 81.01 K. Monitoring point 5 is the farthest from the cold impact wave source, and its temperature decreases the slowest. At t = 4200 s, the temperature at monitoring point 5 dropped to 88.20 K. When the liquid nitrogen cold soaking time is t = 4200 s, the temperature at monitoring point 6 drops to 87.21 K. When the liquid nitrogen cold soaking time is t = 4200 s,

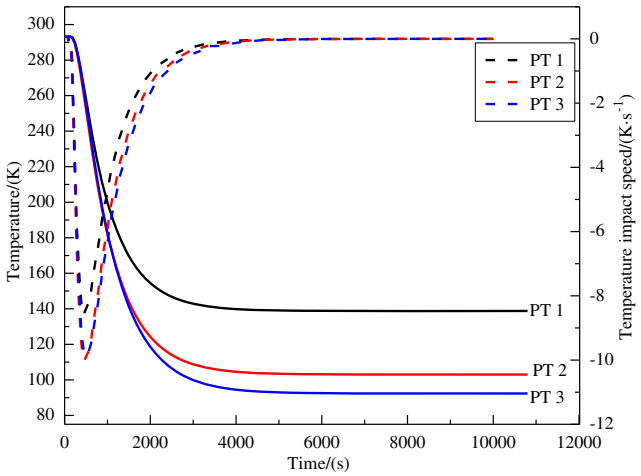

Fig. 6 Variation of coal surface temperature impact speed with liquid nitrogen cold soaking time

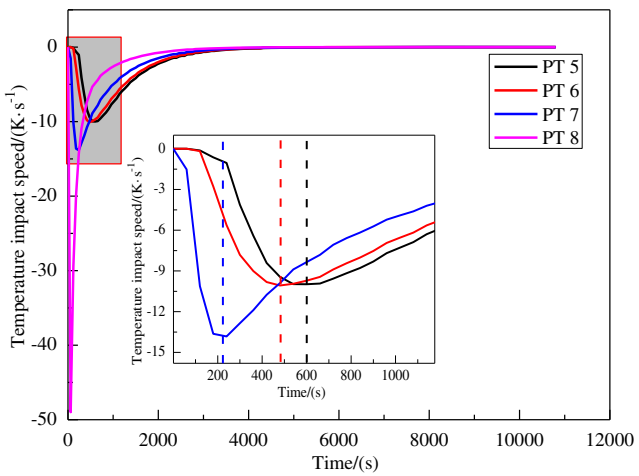

Fig. 8 Radial temperature impact speed of coal with cold liquid nitrogen soaking time

the temperature at monitoring point 7 drops to 84.71 K. The temperatures of the four monitoring points decrease with time and eventually stabilize.

Figure 8 shows the trend of temperature impact speed at monitoring points 5~8 with time. When t = 60 s, the temperature impact speed of monitoring point 8 reaches the maximum amplitude of − 48.99 K/s. When t = 240 s, the temperature impact speed of monitoring point 7 reaches the maximum, and the maximum value is − 13.82 K/s. Monitoring points 5 and 6 reach the maximum temperature impact speed at 600 s and 480 s, respectively. And compared with the maximum temperature impact speed at monitoring point 8, the maximum temperature impact speed at monitoring point 5 is reduced by 79.62%, and the temperature at the monitoring point 6 is reduced by 79.44%. The farther the monitoring point is from the temperature impact source, the larger the amplitude of the temperature impact speed, and the shorter the time required to reach the amplitude. The temperature impact speeds at monitoring points 5~8 all increase first to reach the amplitude, then decrease, and eventually stabilize.

Figure 9 is the temperature gradient change of the internal monitoring points 5~8 of the coal specimen with liquid nitrogen cold soaking and a partial enlarged view. Figure 9 shows that the internal temperature gradients of coal increase first, then decrease and eventually stabilize with the liquid nitrogen soaking time increases. After monitoring, when the initial temperature of coal is 273.15 K, the temperature gradient at monitoring point 5 is at t = 600 s, with a negative maximum, and the maximum value is − 399.26 K/m. The temperature gradient of monitoring point 6 reaches the negative maximum (− 537.04 K/m) at t = 480 s. When t = 240 s, the temperature gradient of monitoring point 7 is negative maximum, and the maximum value is − 1105.58 K/m. Monitoring point 8 is closest to the low-temperature liquid nitrogen surface, and at t = 60 s, a temperature gradient of − 7837.87 K/m is instantaneous. As the liquid nitrogen cold soaking time continues to increases, the temperature gradient gradually decreases and eventually stabilizes.

In summary, the overall temperature change curve of the coal specimen during the liquid nitrogen cold soaking can be divided into three stages: the first stage is the temperature acceleration change stage, that is, the temperature acceleration decreases and the temperature gradient increases linearly to the peak with time. The second stage is the temperature deceleration change stage, that is, the temperature deceleration decreases and the temperature gradient decreases with time from the peak value to zero. The third stage is the temperature stabilization stage, that is, the temperature no longer changes, the temperature gradient is zero, and the temperature equilibrium stable state is reached.

Comparison of experimental results and numerical simulation results of coal surface temperature under the liquid nitrogen cold soaking

The temperature sensor is inserted into a pre-made borehole (bore diameter 0.006 m, depth 0.055 m), and the temperature change law of the coal specimen is recorded in real time during the liquid nitrogen cold soaking through a multi-channel data recorder and a computer link. Figure 10 is the temperature comparison at the drill hole bottom of coal specimen with time obtained by numerical simulation under the liquid nitrogen cold soaking. When t < 1200 s, the temperature of coal specimens decreases rapidly with the increase of liquid nitrogen cold soaking time. When t = 1200 s, the simulated coal specimen temperature is 172.95 K, and the coal specimen experimentally measured temperature is 170.35 K. When 1200 s < t < 4800 s, the temperature of the coal specimen slows down with the increase of the liquid nitrogen cold soaking time. When t = 4800 s, the simulated coal specimen temperature is 96.04 K, and the coal specimen experimentally measured temperature is 99.15 K. When t > 4800 s, both the

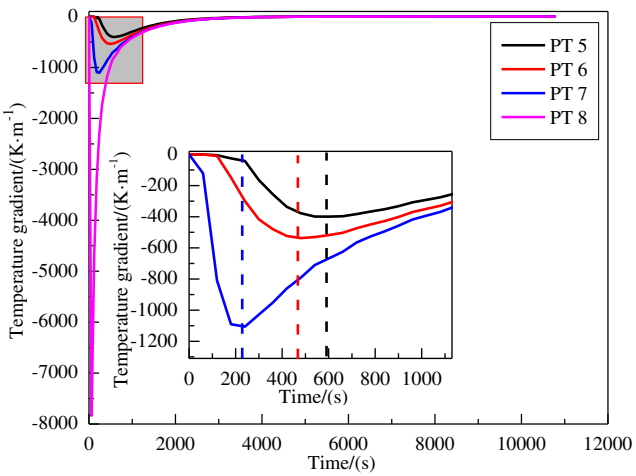

Fig. 9 Temperature gradient with the liquid nitrogen cold soaking time

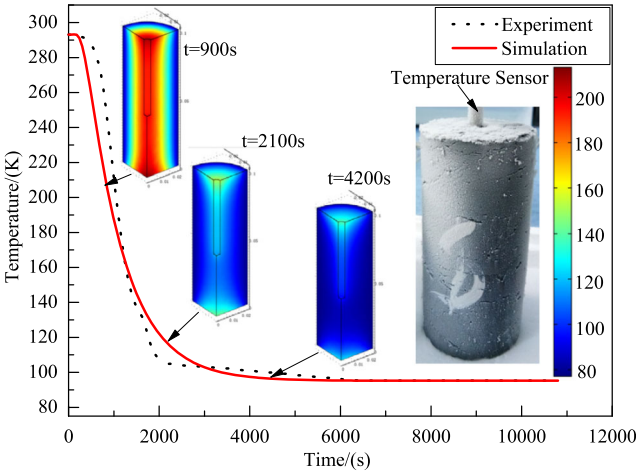

Fig. 10 Experimental and simulation results of coal surface temperature impact speed with the liquid nitrogen cold soaking time

simulated coal specimen temperature and the coal specimen experimentally measured temperature maintaine a stable state. From the three-dimensional simulation results, it is intuitively seen that the low-temperature liquid nitrogen propagates in the form of waves to the center of the coal specimen. When t = 900 s, the central temperature of the coal specimen is still higher than the coal wall temperature. With the increase of liquid nitrogen cold soaking time, the entire coal specimen is gradually assimilated by low-temperature liquid nitrogen, that is, the entire coal test piece maintains a low-temperature state. From the change trend of the coal specimen temperature with time during the liquid nitrogen cold soaking, the numerical simulation is consistent with the laws obtained by laboratory experiments. Therefore, it shows that the model can fully reflect the temperature field change of coal during the liquid nitrogen cold soaking.

Conclusion

Based on the law of energy conservation, the transient temperature field equation of coal specimens under the liquid nitrogen cold soaking was obtained. The COMSOL numerical simulation platform was used to numerically simulate the temperature conduction of coal specimens, and the temperature field evolution law of coal specimens during the liquid nitrogen cold soaking was analyzed in detail. The following main research conclusions were obtained:

(1) Based on the heat conduction theory, the heat conduction equation of coal during the liquid nitrogen cold soaking is obtained. The temperature and space changes of coal under the liquid nitrogen cold soaking are numerically simulated with the COMSOL software platform.
(2) The temperature field of coal under the liquid nitrogen cold soaking propagates from outside to inside in the form of temperature impact wave. The temperature impact wave gradually decays with the increase of the propagation distance. The temperature of coal specimens decreases as a negative logarithmic function with the increase of liquid nitrogen cold soaking time. The temperature curve can be divided into three phases: accelerated descent, decelerated descent, and maintaining stability. The closer the inside of the coal specimen is to the liquid nitrogen boundary surface, the greater the temperature impact speed and temperature gradient, and the shorter the time required to reach a steady state.
(3) Taking a dry coal specimen (Φ 0.05 m × 0.1 m) with a diameter of 0.006 m and a depth of 0.055 m as an example, the laboratory test results and numerical simulation results are compared. The results show that the evolution laws of the temperature field inside and on the surface of the coal specimen under the liquid nitrogen cold soaking have a good consistency, which verifies the rationality of the numerical analysis.

In future research on the temperature field of coal and rock, the influence of thermal conductivity and ice water phase transition on the temperature field distribution and internal morphology of coal and rock during liquid nitrogen cold soaking should be considered.

Funding The authors would like to acknowledge the financial support from National Natural Science Foundation of China (Grant Number: 51774118), the State Key Laboratory Cultivation Base for Gas Geology and Gas Control (Henan Polytechnic University) (Grant Number: WS2019B02), Natural Science Foundation of Chongqing, China (Grant Number: cstc2019jcyj-bsh0041), the Postdoctoral Science Foundation Project Funded by State Key Laboratory of Coal Mine Disaster Dynamics and Control (Grant Number: 2011DA105287-BH201903), and the Chinese Ministry of Education Innovation Team Development Plan (Grant Number: IRT_16R22).

Compliance with ethical standards

Conflict of interest The authors declare that they have no conflict of interest.

References

Benaceur K, Stephenson P (2010) Models of heat transfer in hydraulic fracturing. Int J Numer Methods Eng 24(1):75–87
Bronfenbrenerb L (2009) The modeling of the freezing process in fine-grained porous media: application to the frost heave estimation. Cold Reg Sci Technol 56(2):130–134
Cai C, Gao F, Li G, Huang Z, Hou P (2016) Evaluation of coal damage and cracking characteristics due to liquid nitrogen cooling on the basis of the energy evolution laws. Journal of Natural Gas Science and Engineering 29(2):30–36
Cha M, Yin X, Kneafsey T, Johanson B, Alqahtani N, Miskimins J, Patterson T, Wu Y (2014) Cryogenic fracturing for reservoir stimulation – laboratory studies. J Pet Sci Eng 124(12):436–450
Chaudhary G, Li R (2014) Freezing of water droplets on solid surfaces: an experimental and numerical study. Exp Thermal Fluid Sci 57(3): 86–93
Coetzee S, Neomagus HWJP, Bunt JR, Strydom CA, Schobert HH (2014) The transient swelling behavior of large (−20 +16 mm) South African coal particles during low-temperature devolatilisation. Fuel 136(10):79–88
Guo JC, Liu YX (2014) A comprehensive model for simulating fracturing fluid leakoff in natural fractures. Journal of Natural Gas Science and Engineering 21(11):977–985
Hebblewhite B, Galvin J (2017) A review of the geomechanics aspects of a double fatality coal burst at Austar Colliery in NSW, Australia in April 2014. Int J Min Sci Technol 27(1):3–7
Holman JP (1990) Heat Transfer, 7th edn. McGraw-Hill Publishing Company, New York
Huang J, Griffiths DV, Wong SW (2012) Initiation pressure, location and orientation of hydraulic fracture. Int J Rock Mech Min Sci 49(1):59–67
Incropera FP, DeWitt DP (1996) Fundamentals of heat and mass transfer, 4th edn. John Wiley and Sons, New York
Karacan C, Ruiz FA, Cotè M, Phipps S (2011) Coal mine methane: a review of capture and utilization practices with benefits to mining

safety and to greenhouse gas reduction. Int J Coal Geol 86(2-3): 121–156
Kong XG, Wang EY, Li SG, Lin HF, Xiao P, Zhang KZ (2019) Fractals and chaos characteristics of acoustic emission energy about gas-bearing coal during loaded failure. Fractals 27(5):1950072
Kong XG, Wang EY, Li SG, Lin HF, Zhang ZB, Ju YQ (2020) Dynamic mechanical characteristics and fracture mechanism of gas-bearing coal based on SHPB experiments. Theor Appl Fract Mech 105: 102395
Li Z, Xu H, Zhang C (2016) Liquid nitrogen gasification fracturing technology for shale gas development. J Pet Sci Eng 138(2):253–256
Li X, Li Z, Wang E, Liang Y, Li B, Chen P, Liu Y (2018) Pattern recognition of mine microseismic (MS) and blasting events based on wave fractal features. Fractals 26(3): 1850029-1-1850029-18.
Lin B, Liu T, Zou Q, Zhu C, Yan F, Zhang Z (2015) Crack propagation patterns and energy evolution rules of coal within slotting disturbed zone under various lateral pressure coefficients. Arab J Geosci 8(9): 6643–6654
Liu XF, Song DZ, He XQ (2019) Nanopore structure of deep-burial coals explored by AFM. Fuel 246:9–17
Liu SM, Li XL, Wang DK, Wu MY, Yin GZ, Li MH (2020a) Mechanical and acoustic emission characteristics of coal at temperature impact. Nat Resour Res 29(6):1755–1772
Liu S, Wang D, Yin G, Li M, Li X (2020b) Experimental study on the microstructure evolution laws in coal seam affected by temperature impact. Rock Mech Rock Eng 53(3):1359–1374
Lu J, Yin G, Deng B, Zhang W, Li M, Chai X, Liu C, Liu Y (2019) Permeability characteristics of layered composite coal-rock under true triaxial stress conditions. Journal of Natural Gas Science and Engineering 66(6):60–76
Mark C, Gauna M (2016) Evaluating the risk of coal bursts in underground coal mines. Int J Min Sci Technol 26(1):47–52
Mcdaniel BW, Grundmann SR, Kendrick WD (1997) Field applications of cryogenic nitrogen as a hydraulic fracturing fluid. J Pet Technol 50(3):561–572
McDermott CI, Randriamanjatosoa ARL, Tenzer H, Kolditz O (2006) Simulation of heat extraction from crystalline rocks: the influence of coupled processes on differential reservoir cooling. Geothermics 35(3):321–344
Mitra A, Harpalani S, Liu S (2012) Laboratory measurement and modeling of coal permeability with continued methane production: part 1 – laboratory results. Fuel 94(8):110–116
Moore T (2012) Coalbed methane: a review. Int J Coal Geol 101(1):36–81
Mottaghy D, Rath V (2006) Latent heat effects in subsurface heat transport modelling and their impact on palaeotemperature reconstructions. Geophys J R Astron Soc 164(1):236–245
Park C, Synn JH, Shin HS, Cheon DS, Lim HD, Jeon SW (2004) Experimental study on the thermal characteristics of rock at low temperatures. Int J Rock Mech Min Sci 41(3):367–368
Perera MSA, Ranjith PG (2012) Carbon dioxide sequestration effects on coal's hydromechanical properties: a review. Int J Energy Res 36(10):15–31
Qin L, Zhai C, Liu S, Xu J (2017) Changes in the petrophysical properties of coal subjected to liquid nitrogen freeze-thaw–a nuclear magnetic resonance investigation. Fuel 194(15):102–114
Ramey JHJ (1962) Wellbore heat transmission. J Pet Technol 14(4):427–435
Settari A, Cleary MP (1984) Three-dimensional simulation of hydraulic fracturing. J Pet Technol 36(8):117–119
Shang D, Yin G, Zhao Y, Deng B, Liu C, Kang X, Lu J, Li M (2018) Local asymmetric fracturing to construct complex fracture network in tight porous reservoirs during subsurface coal mining: an experimental study. Journal of Natural Gas Science and Engineering 59(11):343–353
Shen Y, Yang Y, Yang G, Hou X, Ye W, You Z, Xi J (2018) Damage characteristics and thermo-physical properties changes of limestone and sandstone during thermal treatment from −30 °C to 1000 °C. Heat Mass Transf 54(5):3389–3407
Shi G, Ding P, Guo Z, Wang Y (2019) Modeling temperature distribution upon liquid-nitrogen injection into a self heating coal mine goaf. Process Saf Environ Prot 126(6):278–286
Shu C, Wang H, Li X, Fan J, Ye X (2020) A thermo-hydro-mechanical model: capturing the effects of initial permeability and gas pressure on outburst-prone indicators. Nat Resour Res 29(10):1897–1914
Tan X, Chen W, Tian H, Cao J (2011) Water flow and heat transport including ice/water phase change in porous media: numerical simulation and application. Cold Reg Sci Technol 68(1):74–84
Taron J, Elsworth D, Min KB (2009) Numerical simulation of thermal-hydrologic-mechanical - chemical processes in deformable, fractured porous media. Int J Rock Mech Min Sci 46(5):842–854
Vitelv M, Rouabhir A, Tijani M, Guérin F (2015) Modeling heat transfer between a freeze pipe and the surrounding ground during artificial ground freezing activities. Comput Geotech 63(1):99–111
Wang D, Yao B, Gao Y, Li W, Lv R (2017) Effect of cyclic temperature impact on coal seam permeability. Therm Sci 21(S1):351–357
Xue YC, Sun WB, Wu QS (2020) The influence of magmatic rock thickness on fracture and instability law of mining surrounding rock. Geomechanics and Engineering. https://doi.org/10.12989/gae.2020.20.6.000
Yang GS (2001) Analysis of the mechanic characteristics of the damage propagation of rock under triaxial stress condition. International Journal of Coal Science and Technology 7(1):35–38
Yang XL, Wen GC, Dai LC (2019) Ground subsidence and surface cracks evolution from shallow-buried close-distance multi-seam mining: a case study in Bulianta coal mine. Rock Mech Rock Eng 52(8):2835–2852
Yin G, Li M, Wang J, Xu J, Li W (2015) Mechanical behavior and permeability evolution of gas infiltrated coals during protective layer mining. Int J Rock Mech Min Sci 80(12):292–301
Zhang S, Tang S, Qian Z, Pan Z, Guo Q (2014) Evaluation of geological features for deep coalbed methane reservoirs in the Dacheng Salient, Jizhong Depression, China. Int J Coal Geol 133(11):60–71
Zhang X, Sun P, Yan T, Huang Y, Ma Z, Zou B, Zheng W (2015) Water's phase diagram: from the notion of thermodynamics to hydrogen-bond cooperatively. Prog Solid State Chem 43(3):71–81
Zhang R, Liu J, Sa ZY (2020) Fractal characteristics of acoustic emission of gas-bearing coal subjected to true triaxial loading, Measurement, 10.1016/j.
Zhou F, Sun WB, Shao JL (2020) Experimental study on nano silica modified cement base grouting reinforcement materials. Geomechanics and Engineering 20(1):67–73